Photocatalytical Properties of TiO$_2$ Nanotubes

Hai-chao Liang[1], Xiang-zhong Li[1,*], Janusz Nowotny[2,**]

[1] *Department of Civil and Structural Engineering, The Hong Kong Polytechnic University, Hong Kong, China.*

[2] *Solar Energy Technologies, University of Western Sydney, Penrith South DC NSW 1797, Australia*

Corresponding author (*). Tel.: +852-2766-6016; Fax: +852- 2334-6389.

E-mail address: cexzli@inet.polyu.edu.hk.

Abstract

Titanium dioxide (TiO$_2$) nanotubes have been reported one decade ago and have proven to be of a great interest in photocatalytic water splitting, as well as gas sensing and anti-bacterial/cancer treatment. This paper presents an overview on general preparation approaches (chemical treatment, template method and anodic oxidation) of tubular TiO$_2$ nanoarchitectures and their characterization. Current applications of the nanotubes as photocatalysts are also reviewed.

1. Introduction

Since the discovery of photocatalytic water splitting on titania (TiO$_2$) by Fujishima and Honda in 1972, the interest in TiO$_2$ as a photocatalyst for purification of groundwater and wastewater is growing [1-6]. The effective photoexcitation of TiO$_2$ photocatalysts requires the application of light with energy higher than its band-gap energy [7,8], thus resulting in the formation of electrons (e$^-$) in the conduction band

1

and positive holes (h^+) in the valence band. Excited state electrons and holes can recombine and then dissipate the input energy as heat, get trapped in metastable surface states, and react with electron donors/acceptors. If a suitable reductant (electron donor) or oxidant (electron acceptor) is available to trap the hole or electron, recombination is prevented and subsequent photocatalytic reactions may occur efficiently on the semiconductor surface. Actually, photocatalytic reactions may occur by either directly via the valence-band hole or indirect oxidation via the surface-bound hydroxyl radicals (i.e., a trapped hole at the particle surface reacts with HO^- or H_2O to be transformed into •OH) [9]. The •OH radicals produced by TiO_2 are one of the most powerful oxidizing species with an oxidation potential of 2.80 V [10,11]. Unlike other radicals, hydroxyl radicals are non-selective and thus readily attack a large group of organic chemicals to be hydroxylated or form partially oxidized intermediates. At sufficient contact time and proper operation conditions, it is practically possible to mineralize the target pollutants to CO_2. The remarkable advantage of semiconductor photocatalysis over all chemical and biological processes is that they are totally ''environmentally friendly'' as they neither transfer pollutants from one phase to the other (as in chemical precipitation, adsorption and volatilization) nor produce massive amounts of hazardous sludge [12].

In this general mechanism, electron transport is a limiting factor in the photocatalytic performance of TiO_2 materials, while the structure of TiO_2 is a crucial factor in the influence of electron transport. The structural disorder at the contact between two crystalline nanoparticles leads to enhanced scattering of free electrons, thus reducing electron mobility [13]. In contrast, an ordered and strongly interconnected nanoscale architecture offers the potential for improved electron transport leading to higher photoefficiency. This has resulted in one-dimensional TiO_2 materials, such as nanowires, nanorods and hollow nanotubes, receiving a great deal of attention in recent

years [14,15]. Among these materials, hollow TiO_2 nanotubes that have surface area-related properties can further improve photocatalytic properties because they demonstrate a superior electron transport.

2. Definition of TiO_2 nanotubes

TiO_2 nanotubes (TNTs) are tubular nanomaterials and exhibit unusual strength, unique optical properties and interesting semiconducting properties. The defined geometry results in special diffusion paths not only for entering the tubular depth (e.g., reactants to be transported into tubes) but also for species to be transported through the tube wall (e.g., electrons, holes and ions). Also, the hollow structure can potentially enhance electron percolation and light conversion, as well as the improved ion diffusion at the semiconductor-electrolyte interface [14,16]. Therefore, the nanotubular TiO_2 materials are expected to great potential applications in electronics, optics, catalysis, energy storage/conversion, and biomedicine. A timeline showing the development and application of TNTs is shown in Fig. 1.
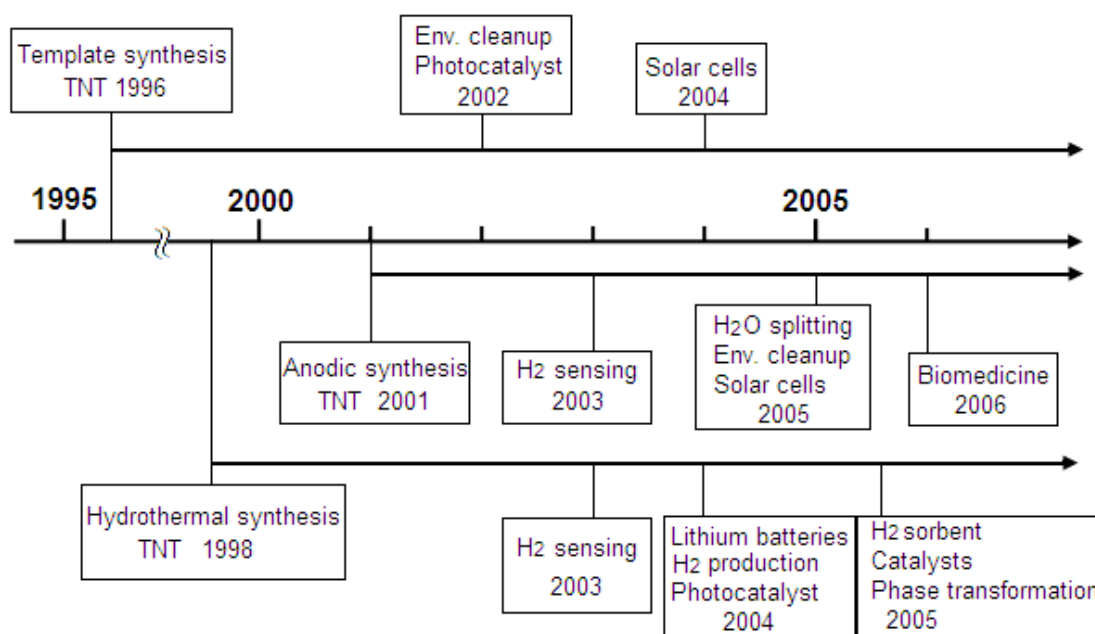

Figure 1. Timeline describing the development of TiO_2 nanotubular structures.

Due to the wide range of applications, the feasibility to produce self-organized TNT nanostructures has received huge scientific and also significant technological interest. In this paper, we therefore attempt to give an overview of some of the underlying principles governing TNT-photocatalysis (the known properties and surface modifications) and to review the current literature in terms of potential environmentally friendly applications.

2. Fabrication of TNTs

To date considerable efforts have been devoted to the preparation of various nanotubular TiO_2 catalysts by mainly the template-assisted method, chemical treatments of fine TiO_2 particles and electrochemical anodic oxidation of pure titanium sheet. There are respective advantages and limitations in each of the above-mentioned methods.

2.1 Alkaline hydrothermal synthesis

TiO_2 nanotubes can be easily fabricated by hydrothermal treatment of crystalline TiO_2 (anatase, rutile, brookite or their mixture) with highly concentrated NaOH. This method generally produces the nanotubes as small as 10 nm (see Fig. 2) and can derivate different crystal structures apart from the formation of anatase TiO_2 nanotubes. For example, some titanate structures, such as $A_2Ti_2O_5 \cdot H_2O$ [18], $A_2Ti_3O_7$ [19], $H_2Ti_4O_9 \cdot H_2O$ [20], and lepidocrocite titanates [21], have been assigned as nanotube constituents (A = Na and/or H). Such discrepancy demonstrates the need for further investigation on this subject although many groups have tried to analyze the structure of the resulting nanotubes. The mechanism of nanotube formation is also under debate, however, there is a common agreement that after breaking of chemical bonds in the

starting tridi- mensional TiO_2 structure, layered entities (2-D) are formed and converted into nanotubes (1-D) through a sheet folding mechanism [22,23].
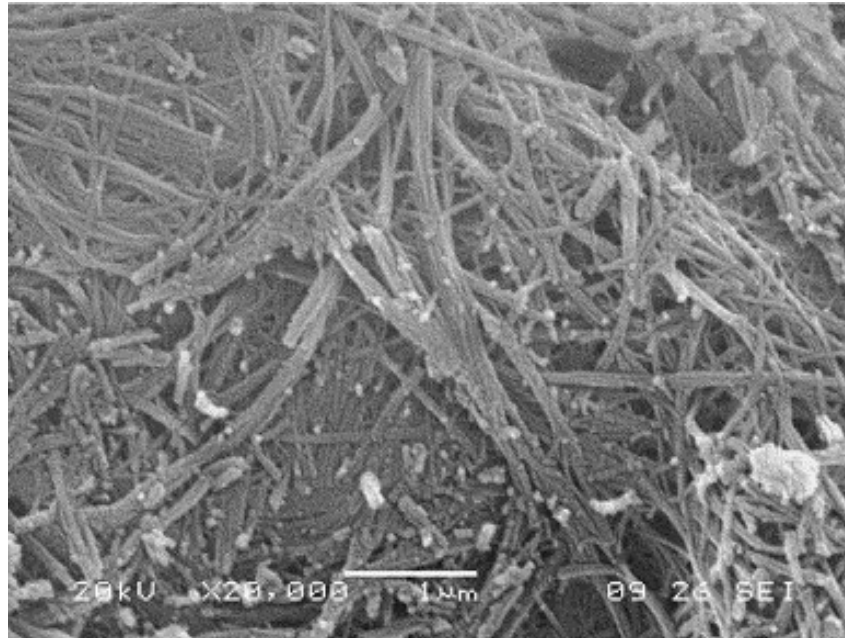

Figure 2. SEM image of the hydrothermal-synthesized nanotube product. Reprinted from ref [17]. Copyright 2006 Elsevier.

On the other hand, it is widely recognized that the NaOH treatment and post-treatment washing seem to significantly affect the formation and transformation of nanotubes. Knowledge of this transformation could significantly extend the application of this specifically featured material. Table 1 summarizes the nanotube structures proposed by different preparation conditions, which generally involved NaOH treatment, followed by post-treatment washing. The data suggest that the post-treatment was a critical step for nanotube formation. For example, Nakahira et al. [20] characterized the hydrothermal TNT sample as a tetratitanic acid $H_2Ti_4O_9 \cdot H_2O$. However, Jin and co-workers [18] proposed the following crystal structure of titanate nanotubes: $H_2Ti_2O_4(OH)_2$ with an orthorhombic unit cell. Both protons of the bititanic

acid could be ion exchanged with sodium ions. These results indicate that the acidity in the post-treatment washing plays a key role in determining the structure of the nanotubes.

Table 1. Nanotube structures prepared from different processes [24].

Precursor	NaOH treatment [a]	Post-treatment	Refs.
Nanotube Structure: Anatase TiO$_2$			
anatase	hydro/110/20	HCl + water	[25]
rutile	chem/110/20	HCl + water	[26]
anatase	chem/150/12	water	[27]
anatase	hydro/110/20	HNO$_3$ + water	[28]
anatase/rutile	hydro/130/24	HCl	[24]
Nanotube Structure: Anatase TiO$_2$/H$_2$Ti$_3$O$_7$•0.5H$_2$O			
rutile	chemi/110/4[b]	HNO$_3$ + water	[29]
Nanotube Structure: A$_2$Ti$_2$O$_5$•H$_2$O			
TiO$_2$ powder	chem/110/20	HCl + water	[30]
anatase	chem/110/20	HCl + water	[18]
Nanotube Structure: A$_2$Ti$_3$O$_7$			
anatase	hydro/130/72	HCl + water	[19]
anatase	hydro/130/72	HCl + water	[31]
any crystals	hydro/130/72	water	[32]
anatase	hydro/180/24	HCl + water	[33]
rutile	hydro/150/72	HCl + water	[23]
Nanotube Structure: H$_2$Ti$_4$O$_9$•H$_2$O			
anatase/rutile	hydro/110/96	HCl + water	[20]
Nanotube Structure: Lepidocrocite Titanates			
anatase	hydro/150/48	HCl + water	[22]

[a] Treatment conditions refer to chemical or hydrothermal processes, temperature (°C) and duration (h), respectively.

[b] Sonication at 280 W before chemical treatment.

2.2 Template-assisted synthesis

Template replication techqniue has been widely used to produce nanoscopic pieces of material in a particular shape [34]. This method utilizes the morphological properties of

characterized template materials to construct other materials with a similar morphology by methods including reactive deposition and dissolution. In principle, this approach is a versatile method for synthesizing nanomaterials with controllable size, morphology and structure. The tubule of the desired material is obtained within the pores of templates. However, the template material has to be sacrificial and generally needs to be removed after synthesis. Anodically formed porous alumina oxide (AAO) usually is used as a template due to the uniform pore size, high pore density together with relative ease of their preparation [35-37]. The synthesis of TNTs by AAO-templating usually involves the sol–gel hydrolysis of Ti^{4+}-containing compounds in the presence of templating agents, followed by deposition of TiO_2 into or onto the template aggregates. Further reaction causes bonds to form between the sol particles and the gel is then typically heated to yield the desired material. In fact, the important part of the tubes is the free space in their interior. It is evident that the size of sol particles is smaller than that of the pore of AAO template for successfully extending into the TiO_2 deposition. However, the irregular deposition and poor penetration of sol particles generally occurs. This is related to the surface charge of sol particles, when template pores establish surface charges impeding sol particles entering the pores. The next stage is selective removal of the templating agent. The AAO template can be partially or completely removed by chemical etching with acid or alkaline. After selective removal of alumina, the external diameter of the TiO_2 hollow fibers corresponds to the diameter of the pores in the alumina.

It is worth noting that by the sol-gel template method, generally the tubular and fibrillar nanostructures within the template pores can be synthesized simultaneously and even an ensemble of nanostructures that protrude from a surface like the bristles of a brush could also be obtained [38]. For example, Martin and co-workers [39] reported that TNTs were obtained if the membrane is immersed into the sol for a brief period (5

s, Fig. 3a), whereas solid TiO$_2$ fibrils were obtained after long immersion times (60 s, Fig. 3c). Intermediate immersion times yield tubules with very thick walls (25 s, Fig. 3b).
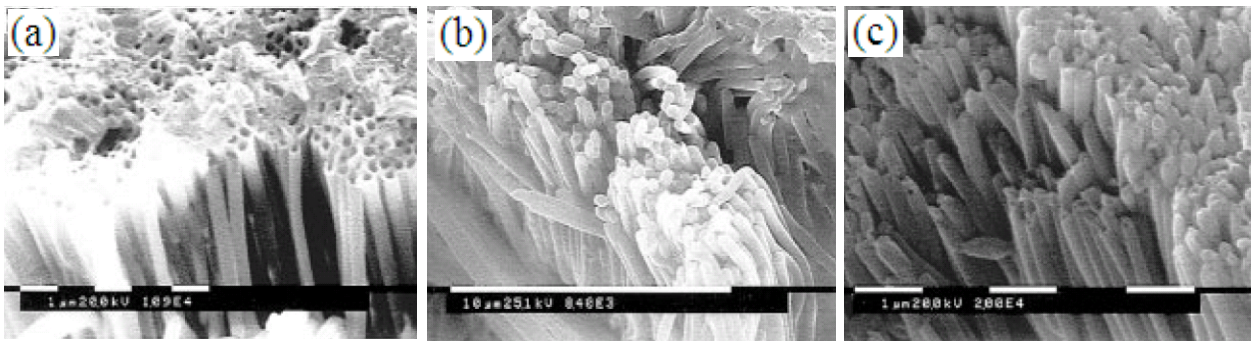

Figure 3. SEM images of TiO$_2$ tubes and fibrils prepared in the alumina membrane. The sol was maintained at 15 °C, and the immersion time was varied from 5 to 60 s. (a) Immersion time) 5 s; (b) Immersion time) 25 s; (c) Immersion time) 60 s. Reprinted from ref [39]. Copyright 1997 American Chemical Society.

2.3 Anodic oxidation process

In 1991, Zwilling et al. [40] first reported the porous surface of TiO$_2$ films electrochemically formed in fluorinated electrolyte by titanium anodization. A decade later Grimes and co-workers [41] synthesized the uniform and highly-ordered TNT arrays by anodic oxidation of a pure titanium sheet in a hydrofluoric acid (HF) aqueous electrolyte. The obtained nanotubes directly grew on the Ti substrate and were oriented in the same direction perpendicularto the surface of the electrode, forming a highly ordered nanotube-array surface architecture.
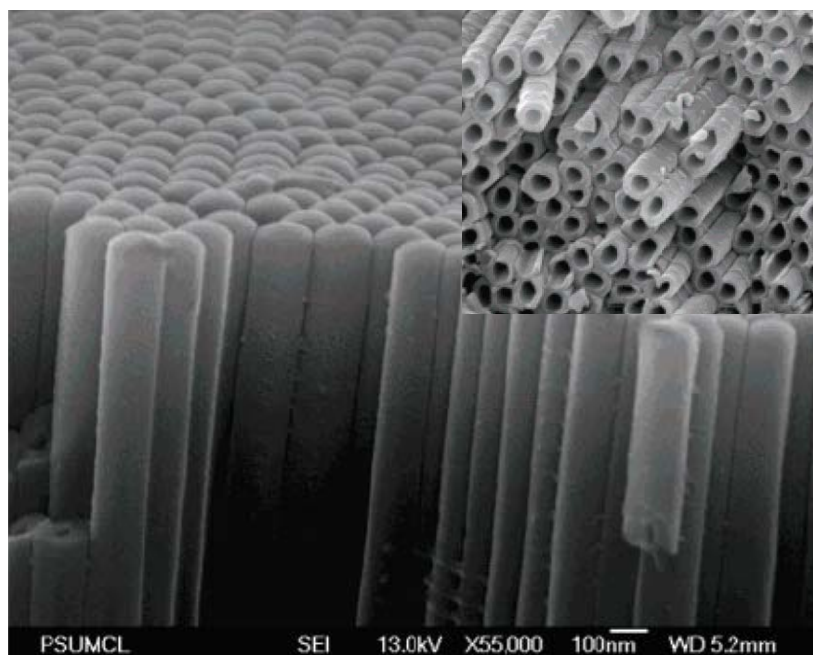
Figure 4. FESEM cross-sectional images of TNT samples. Sample was fabricated at 60 V in 0.25 wt % NH4F ethylene glycol solution. Reprinted from ref [45]. Copyright 2006 American Chemical Society.

In the anodic oxidation process, the electrolyte composition is a critical determinant with regard to the resulting surface morphology, and hence properties of the anodic films. Besides the above-mentioned HF/H_2O electrolyte, other aqueous electrolytes ($KF/NaF/H_2O$, NH_4F/CH_3COOH and NH_4F/H_3PO_4, etc) and nonaqueous electrolytes (fluorinated dimethyl sulfoxide (DMSO)/ethanol, NH_4F/glycerol, etc) have been developed to prepare TNT arrays [42-45]. In aqueous electrolytes, the length of obtained nanotube arrays is usually less than 500 nm while in nonaqueous organic polar electrolytes, TiO_2 nanotubes can reach a 134 μm of length and generally have a smooth outer tubewall (see Fig. 4).

To have a better understanding in anodic TNTs, Mor et al. [16] proposed a mechanistic model for the nanotube array formation, as shown in Fig. 5. With the onset

of anodization, a thin oxide layer is developed on the titanium surface (Fig. 5a) and then undergoes the localized dissolution to form small pits (Fig. 5b). The localized dissolution behavior not only produces a thinner barrier layer at the bottom of the pits but also permits the barrier layer further pore growth (Fig. 5c). The electric field distribution in the curved bottom surface of the pore causes pore widening, as well as the pore deepening. As the pores become deeper the electric field in these protruded metallic regions increases enhancing the field-assisted oxide growth and oxide dissolution, hence simultaneously with the pores well-defined inter-pore voids start forming (see Fig. 5d). Thereafter, both voids and tubes grow in equilibrium. The nanotube length increases until the electrochemical etch rate equals the chemical dissolution rate of the top surface of the nanotubes.
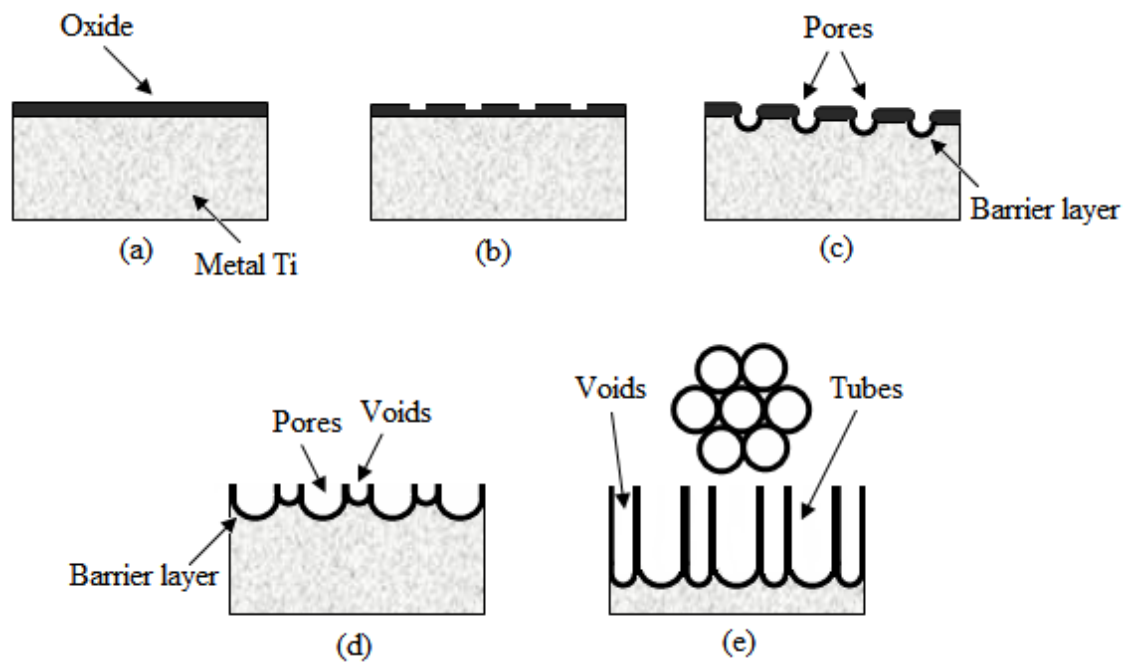

Figure 5. Schematic diagram of the evolution of nanotube arrays at constant anodization voltage: (a) oxide layer formation, (b) pit formation on the oxide layer, (c) growth of the pit into scallop shaped pores, (d) metallic part between the pores undergoes oxidation and field assisted dissolution, and (e) fully developed nanotube

arrays with a corresponding top view. Reprinted from ref [16]. Copyright 2006 Elsevier.

4. Characteristics of TNTs

4.1 Textural properties

It is widely accepted that photocatalytic reactions occur on the surface of catalyst in contact with substrates, where reactant molecules must be first adsorbed by photocatalysts. This indicates that photocatalytic efficiency is significantly influenced by the physicochemical properties of photocatalysts like crystalline structure, surface area, surface acidity, and surface functional groups. Among these factors, a high surface area can be one of the most important factors in certain photocatalytic reactions, as a large adsorption capacity of photocatalysts can promote the reaction rate [46-48]. When compared to TiO_2 powders, TNT catalysts have a higher specific surface area making a higher photoactivity.

Table 2 summarizes the pore structures and special surface area of various TNT catalysts with comparison of Degussa P25 TiO_2. The commercial P25 powder is known to be very fine with a particle size of 25–30 nm, a porous surface of 0.092 pore volume and have a special surface area of ~50 m^2 g^{-1}, while the lab-made TNT catalysts generally present a big difference in these textural properties. For example, the hydrothermal-synthesized TNT samples (TNT-H) the BET specific surface areas range from 200 to 400 $m^2 g^{-1}$, 4-8 times higher than that of P25; pore volume is also significantly greater than that observed for Degussa P25. In addition, these specimens usually have a very small tubewall thickness of 2-3 nm, which can be thought to be a key factor for achieving the higher activity of the nanotube samples due to the feasibility of quantum size effect. Instead of, TNT-T and TNT-A samples show higher BET surface area (usually > 200 $m^2 g^{-1}$) but thicker tubewall (~20 nm). The different

characteristic parameters of these samples to some extent reflect their intrinsic reaction

behavior and respective photocatalytic performance.

Table 2. Comparison of textural properties between various TNTs and Degussa P25.

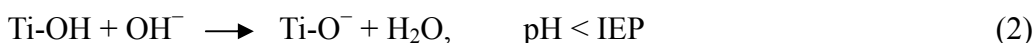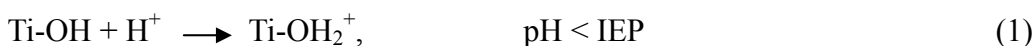| Samples[a]	Pore volume $(cm^3\,g^{-1})$	Pore size (nm)	Thickness (nm)	S_{BET} $(m^2\,g^{-1})$	Ref.
Degussa P25	0.092	8.3	25-30	~50	[49]
TNT- H	0.89	10.3	~2	350.4	[50]
	0.67	6.7	~2	404	[51]
	--	~5	~3	246	[52]
	--	6	~2	200	[53]
TNT-T	0.16	3-11	20-60	95	[54]
	--	50-150	10-20	100-140	[55]
TNT-A	--	20-70	~22	285	[56]

[a] Sample TNT-H, TNT-T and TNT-A was denoted as the material prepared by hydrothermal, template-assisted and anodic techqniue, respectively.

4.2 Surface hydroxyl groups and surface charges

The surface hydroxyl (OH) groups of TiO_2 have been recognized to play an important

role in the photocatalytic behavior, because they not only undertake the adsorption of

reactant molecules but also directly participate in the reaction mechanism by trapping

of photogenerated holes to form hydroxyl radicals [57-59]. However, there are quite

limited reports in the determination of OH groups on the surface of TNTs. In 2006,

Qian et al. [60] investigated the IR spectra of hydrothermally synthesized TNTs. They

suggested that two sharp absorption bands at 1618 and 3423 cm^{-1} were contributed to

the deformation and stretching vibrations of OH group of physisorbed water in TiO_2,

respectively, while the shoulder at 3208 cm^{-1} from Ti–OH bonds was ascribed to the

strong interaction between Ti ions and OH groups. Actually, the defect structure of

TNTs formed by oxygen vacancies favors the adsorption of water on the surface and

then dissociates water into hydroxyl groups and protons [61-63]. This dissociation behavior leads to the charged surface of TNTs due to the loss or gain of protons and complexation reactions of surface hydroxyl groups [64,65]

Electrophoretic mobility is the most common technique for investigating the surface charges of the metal oxide/electrolyte solutions [66,67]. With this technique, the migration of suspended particles is quantified under an electric field. The isoelectric point (IEP) position of TiO_2 depends on the alkali–acid character of surface hydroxyl groups. At the IEP, there are no excess surface charges on TiO_2 and the electrostatic interaction is minimum at this point. The dissociation reactions of surface hydroxyl groups are pH dependent and the acidity of the oxide can be related to the dissociation constants of the reactions. For example, when pH in the aqueous solution is lower than IEP, $Ti\text{-}OH_2^+$ forms and the surface possesses positive charge, while if pH is higher than IEP, $Ti\text{-}O^-$ forms and the surface possesses negative charge (see Eqs. 1 and 2). The lower isoelectric point in terms of the pH value means a higher concentration of hydroxide ions on the surface of the catalyst.

$$Ti\text{-}OH + H^+ \longrightarrow Ti\text{-}OH_2^+, \qquad pH < IEP \qquad\qquad (1)$$

$$Ti\text{-}OH + OH^- \longrightarrow Ti\text{-}O^- + H_2O, \qquad pH < IEP \qquad\qquad (2)$$

A lower isoelectric pH is associated with a more acidic surface, i.e., a higher affinity for protons and a more negatively charged surface. Table 3 listed that the IEP value of P25 presented in many papers is often divergent and mainly ranges from 6.2 to 6.9, while TNTs samples have an IEP value of 5.3-5.5. These results mean that the total amount of hydroxyl groups on the surface of TNTs is higher than that of P25. This hypothesis has been confirmed by comparing the FTIR spectroscopy and surface acidity of P25 and TNT materials [68-70].

Table 3. Comparison of Isoelectric point (IEP) between various TNTs and Degussa P25.

Sample	Isoelectric point	Ref.
Degussa P25	6.2–6.9	[71-73]
TNT-H	5.3–5.5	[74,75]
TNT-T	--	--
TNT-A	~5.3	[76]

4.2 Electrical properties

The photocatalytical properties of TiO_2, including TNT, are closely related to their reactivity and phototoreactivity with water and, in some cases solutes in water. While the reactivity and phototoreactivity are related to the commonly measured properties of photocatalysts, such as surface area, structure, microstructure, and chemical composition, these are determined by the ability of photocatalysts to denote or accept electrons during the photocatalytic reaction. The latter is related by the chemical potential of electrons, μ_e:

$$\mu_e = \mu_e^o + kT \ln[e^-]$$

where μ_e^o denotes μ_e in standard conditions, [e^-] is the concentration of electrons and kT have their traditional meaning.

The key quantities in the characterisation of photoelectrochemical performance of photoelectrochemical devices include the current-voltage characteristics and the efficiency of photocurrent-to-incident photon, E_{ff} (for specific wavelength). The latter may be determined from the following equation:

$$Eff[\%] = \frac{i_{ph}E}{qP}$$

where i_{ph} is photocurrent density, E is photon energy, q is the elementary charge and P is the light density. The plots of E_{ff}^2 vs E for the TNTs at different stages of the formation are presented in Fig. 6. This plot, indicating the effect of the procedure on E_{ff} allows to determine the band gap ($E_g = 3.15$ eV), which appears to be independent of the experimental procedure and the related morphology.
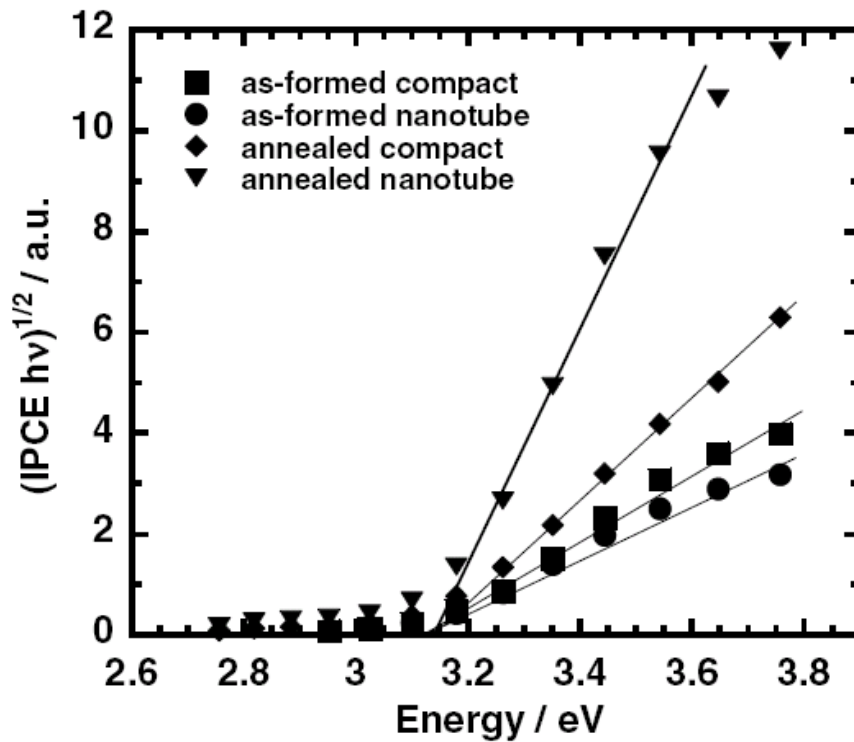

Figure 6. (IPCE hv)$^{1/2}$ vs. hv plots for as-anodized compact and nanotube TiO_2 and annealed nanotube TiO_2. Reprinted from ref [77]. Copyright 2006 Elsevier.

While the measurement of electrical properties done under static conditions (or in equilibrium) that may allow to assess the effect of processing on the concentration of electronic charge carriers (assuming that the mobility term remains constant), the

transient measurement of photocurrent generated under light pulse may be used to assess the life time of the light-induced charge carriers [77].

Essential information concerns the effect of processing on the flat band potential, FBP, which may be determined by the Mott-Schottky formula:

$$\frac{1}{C^2} = \frac{2}{\varepsilon \, \varepsilon_o \, q \, NsubD} (U - U_{FBP} - \frac{kT}{q})$$

where C is the space charge capacitance ($C`` = `` -1/\omega Z''$), ε and ε_o denote the dielectric constant in air and in vacuum, respectively, U and U_{FBP} is the applied potential and the FBP, respectively, N_D is the concentration of donors (for n-type semiconductor), and the kT/q term assumes 25 mV at room temperature. The Mott-Schottky plots for TiO_2 and TNTs (ignoring the capacitance of the Helmholtz layer) are shown in Fig. 7.

In summary, knowledge of electrical properties is essential in the interpretation of photocatalytic properties of TiO_2. The TNT is not an exception.
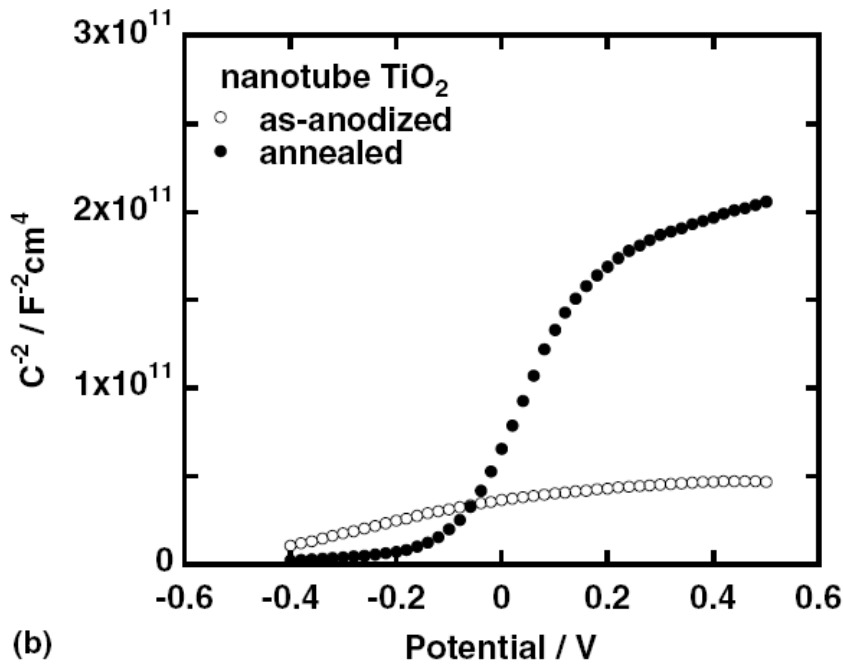

(a)

16
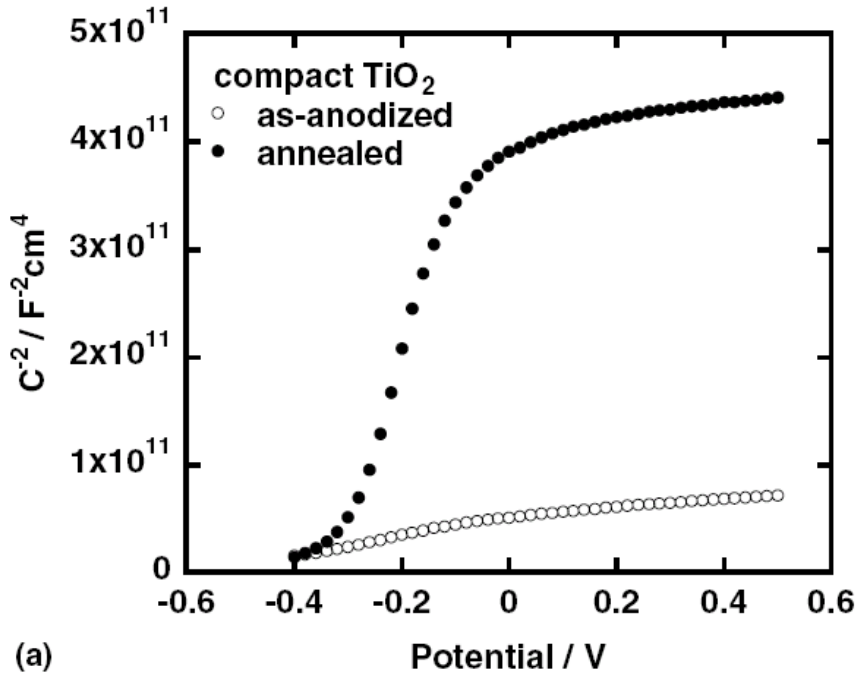
Figure 7. Mott–Schottky plots for (a) compact TiO$_2$ and (b) nanotube TiO$_2$ layer. Reprinted from ref [77]. Copyright 2006 Elsevier.

4.3 Optical properties

TNTs are achieved over a wide range of pore size, wall thicknesses, tube-lengths, and chemical composition, leading to different light absorption and photocatalytic properties [78,79]. The optical behavior of TNTs can be studied by measuring their UV-vis absorption, in which the characteristic absorption band of TNTs should be assigned to the intrinsic transition from the valence band (VB) to the conduction band (CB). In general, the TNT samples exhibit a similar absorption band shape in their UV-vis absorption spectra, as shown in Fig. 8. This phenomenon may be identified to be the sub-band gap states of TNTs due to the special nanotube structure. Their onset absorption always starts from 350-400 nm, corresponding the band gap energy of 3.1-3.5 eV when calculated with Kubelka-Munk function [80].
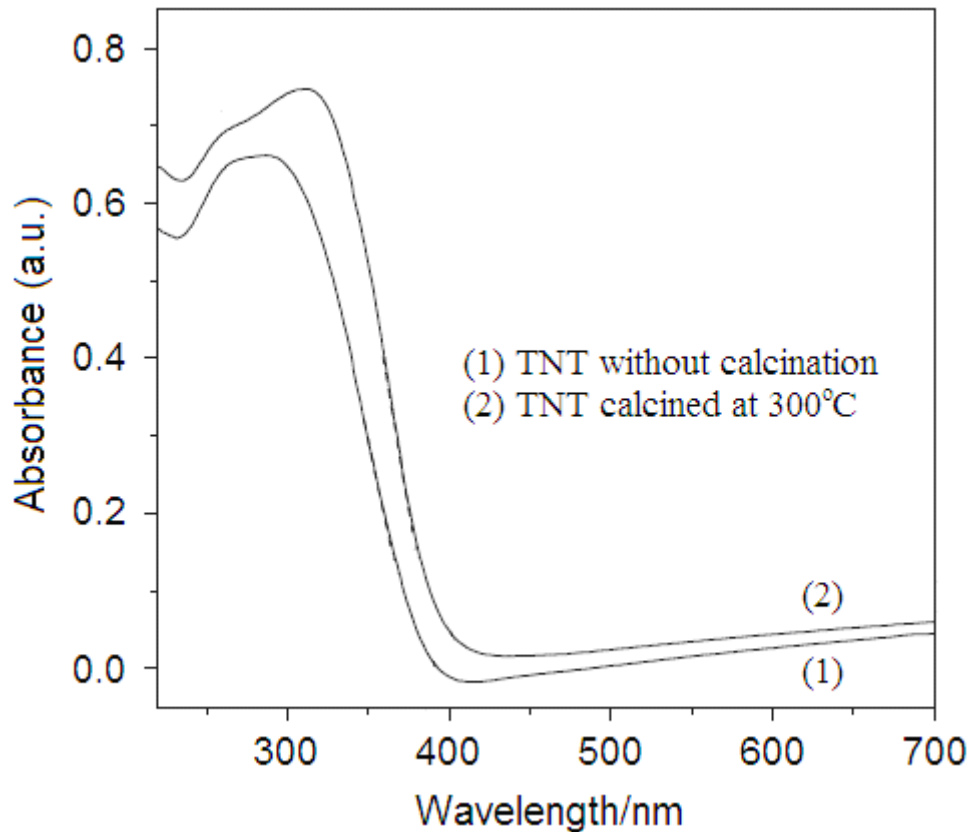
Figure 8. UV-visible absorption spectra of TNTs prepared by hydrothermal treatment. Reprinted from ref [81]. Copyright 2008 Springer.

Table 4 summarizes the onset absorption of TiO_2 P25 and TNTs with corresponding band gap energy. Compared the absorbance of bulk Degussa P25 (at over 400 nm), a blue shift of absorption$_{onset}$ with higher band energy (370-380 nm) for TNTs was clearly observed. The interpretation of the blue-shift is not clear so far. Many have attributed the blue-shift in the TNTs to a quantum-size effect [16,88]. However, others suggest that the absorption blue-shift observed for nanoparticles with diameters > 2 nm may be due to direct interband transitions in this indirect semiconductor [89]. Quan et al. [90] proposed that the significant blue-shift with higher band energy of TNTs compared with the TiO_2 particles may be due to the method of material preparation,

crystal structure and the surface state. Comparison with the theory is difficult and proper understanding of the absorption behavior requires further study.

Table 4. Comparison of UV-vis absorption$_{onset}$ and band gap energy (E_g) between various TNTs and Degussa P25.

Sample	Absorption$_{onset}$ (nm)	E_g^a (eV)	Ref.
Degussa P25	425	2.92	[82]
	400	3.10	[83]
	400	3.10	[84]
TNT-H	~370	3.35	[85]
	~370	3.35	[84]
TNT-T	~370	3.35	[86]
	~375	3.30	[82]
TNT-A	~380	3.26	[77]

[a] The band gap energy (E_g) of materials was calculated according to the equation [87]: $E_g = ch/\lambda \approx 1239/\lambda$, where h is Planck's constant, c is the velocity of light (m/s) and λ is the wavelength of onset absorption (nm).

5. Surface modification of TNTs

Low-dimensional TNTs, since they naturally provide a direct path for electron transport, are suitable for an ideal photocatalyst under irradiation of UV light with wavelength shorter than that corresponding to its band gap energy (> 3.26 eV). However, the photocatalytic process using UV radiation requires substantial electrical power input, leading to the increasing cost and complexity of practical application. From a viewpoint of solar energy utilization, developing photocatalysts capable of using more abundant visible light [4,91,92], which accounts for about 43% of the incoming solar energy, is indispensable.

In recent years considerable effort has been invested in improving the response of TNTs to visible light, mainly including the sensitization with dye [93,94] or polymer [95], loading with noble metal atom [96,97], and coupling with narrow band gap

semiconductor [98,99]. In sensitized cases, charge injection from the CB of the narrowband gap semiconductor to that of TNTs can lead to efficient and longer charge separation by minimizing the electron–hole recombination. In noble metal doping cases, a p-n junction is formed between metal and semiconductor, which results in the decreasing electron–hole recombination and meanwhile produces more oxidizing species to undertake the photocatalysis. Another alternative approach is to couple TNTs by using a narrow band gap semiconductor, which absorbs light in the visible region and may be able to transfer electrons to the large band gap TiO_2 semiconductor. Here, we review various types of modified TNTs so that the material responds more fully to visible light while maintaining the excellent charge transfer properties and chemical stability.

5.1 Dye or polymer-sensitization

Recently, many different sensitizors, including organic dyes and conductive polymers, were widely used in the research of dye-sensitized solar cells (DSSCs) [94,100,101]. This technique can lead to a substantial increase of light-to-electric energy conversion efficiency. Among a wide variety of dyes, polypyridyl complexes of Ru and Os with four pendant carboxyl groups, such as N719 dye (N719 = [tetrabutylammonium]$_2$[Ru(4-carboxylic acid-4'-carboxylate-2,2'- bipyridyl)$_2$(NCS)$_2$]) are the most efficient dyes [93, 102]. In 2007, Zhu et al. [103] found that the TNT-based DSSCs sensitized with N719 dye have a significantly higher light-harvesting efficiency than that of TiO_2 particle-based DSSCs. However, so far there is quite limited literature involving the use of dye-sensitized TNTs as photocatalysts in water treatment due to the nonstability of dye molecules in aqueous environment.

The conjugated polymers as photosensitizors such as polyaniline, polythiophene,

polypyrrole, and their derivatives have shown excellent stability due to their extending π-conjugated electron systems. In a conjugated polymer/TiO_2 system, the polymer, bound to TiO_2, can actively harvest the visible light matching the semiconductor energy levels, and then inject electrons into the conduction band (CB) of TiO_2. A schematic diagram for the charge transfer processes of conjugated polymer and TiO_2 is illustrated in Fig. 9. Here, when the conjugated polymer harvests visible light, an absorbed photon promotes an electron from the ground state of the polymer located in the semiconductor energy gap into an excited state that is in resonance with the CB. The polymer π-orbital becomes the highest occupied molecular orbital (HOMO) in the combined system. Since the lowest unoccupied molecular orbital (LUMO) levels of the polymer are energetically higher than the conduction band edge of TiO_2 [104,105], the electron transfer paths in Fig. 9 are possible. Efficient electron injection into the edge of the CB avoids the energy loss by relaxation to the CB edge [106]. As a result, it should be a vital prerequisite for photosensitization that the interfacial charge transfer between the photosensitizer and the semiconductor takes place, being capable of responding to visible light.
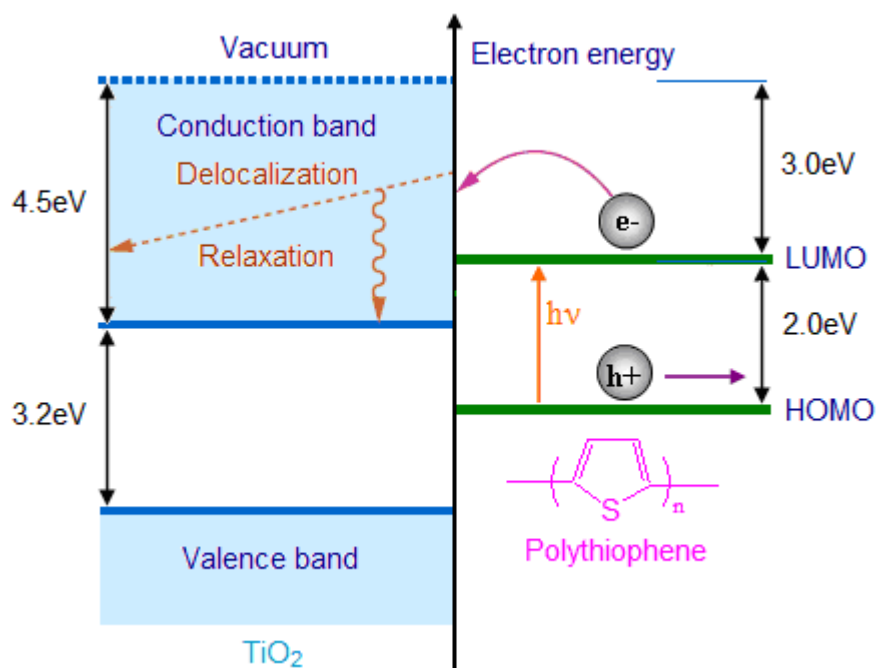
Figure 9. Schematic diagram of conjugated polymer/TNT nanocomposites; detailed view on the polymer-TiO₂ junction and free charge carrier photogeneration mechanism is shown. The conjugated polymer is denoted as polythiophene in the present paper.

5.2 Semiconductor coupling

Semiconductor coupling is another method to utilize visible light for TiO₂ photocatalysis. When a large bandgap TiO₂ semiconductor is coupled with a small bandgap semiconductor with a more negative conduction band level, CB electrons can be injected from the small bandgap semiconductor into the TiO₂ semiconductor. This mechanism is similar to that of dye/polymer-sensitized TiO₂ system (see Fig. 9). Since CdS has narrow bandgap (2.4 eV) and its conduction band is ca. 0.5 eV more negative than that of TiO₂ [98], the coupling of the semiconductor should have a beneficial role not only in sensitizing TiO₂ to visible photoresponse but also in improving charge separation. Early studies concentrated on the formation of CdS/TiO₂ combination by depositing CdS microcrystals (4–20 nm) onto TiO₂ particles or highly porous thin films [107-109]. Recently, CdS/TiO₂ nanotubes were successfully prepared using layer-by-

layer deposition [110], chemical bath deposition [111] and electrodeposition methods [98]. For example, Hsu et al. [111] synthesized a novel CdS@TNT coaxial nanocables using wet chemical bath deposition with porous AAO as templates (see Fig. 10). Using this method, the thickness of the TNT sheaths could be controlled precisely by adjusting the reaction conditions. Sequentially, the continuous and polycrystalline CdS nanotubes were deposited onto TNTs by in order to form the coaxial CdS@TNT nanocables. The capability to construct composite nanotubes with functional interior and exterior layers is an important progress.
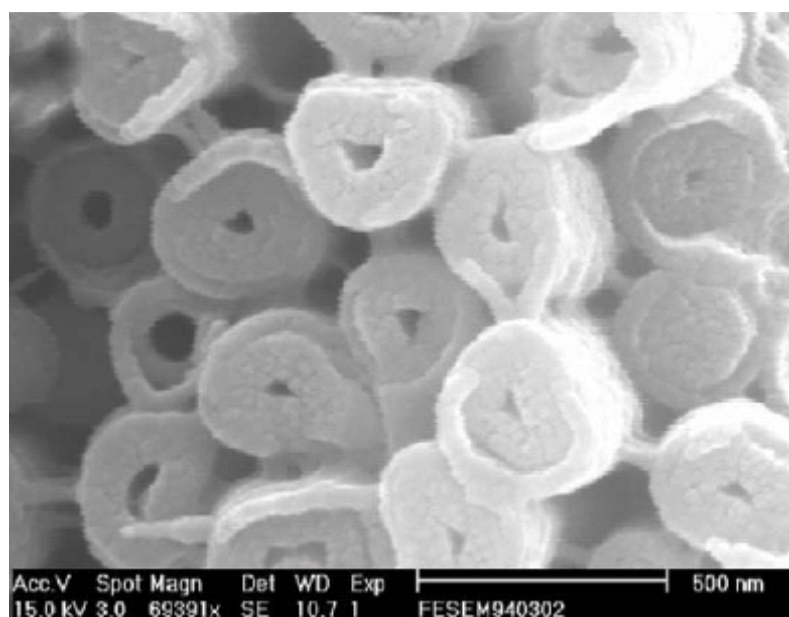

Figure 10. SEM images of CdS@TNT at high magnification. Reprinted from ref [111]. Copyright 2005 Elsevier.

In 2007, Hou and co-workers [99] fabricated a core/sheath heterostructure CdS/TNT electrode by ac electrodeposition of CdS to anodic TNT arrays and used them in photoelectrochemical cells. The core/sheath architecture enhances the photocurrent and efficiency of water photocleavage by allowing for more contact areas of CdS and TNTs.

In this case, charge collection efficiency and light harvesting efficiency may be higher than in a planar heterojunction, which will result in higher cell efficiency.

As we know, the key point of the efficient photocatalysis for TiO$_2$ catalyst is the combination of carrier generation by light absorption and charge separation. In the case of CdS coupling, researchers seek to combine the excellent photochemical properties of the crystalline TNTs with the excellent visible absorption properties of CdS nanoparticles, thereby shifting the absorption characteristics of the material architecture into the visible light spectrum. Unfortunately, photocatalysis with CdS/TiO$_2$ still cannot be applied in real water treatment because of the easy photocorrosion of CdS and its high toxicity.

5.3 Noble metal deposition

Other research efforts related to the deposition of noble metals (mainly include Pt, Pd, Au, and Ag) in/on TNT structures has been in progress. A considerable increase of the photocatalytic activity have been reported, in particular, with platinum deposited on TNTs for water splitting and degradation of organic pollutants [96,97,112]. The deposition of Pt metal on n-type TiO$_2$ semiconductor is similar to those semiconductor-semiconductor p-n junctions [14]. At a p–n junction of Pt/TiO$_2$ system, electrons diffuse from the TiO$_2$ (n-type) into the Pt (p-type) region, creating an accumulation of negative charges in the p-type region in the vicinity of the junction. Simultaneously, holes diffuse from the p-type to the n-type region, creating a positive section in the n-type region in the vicinity of the junction. For this situation, the Pt metal must have a higher work function (5.6 eV) than that of the TiO$_2$ semiconductor (~3.9 eV) [8,113], which renders to form a Schottky barrier between the metal and semiconductor. Fig. 11 schematically illustrates the electron capture properties at the Schottky barrier of the metal in contact with a semiconductor surface. When the two species come in contact

the Fermi levels of the metal and semiconductor align causing electrons to flow to the metal from the semiconductor. The decrease in electron density within the semiconductor causes the holes to freely diffuse to the semiconductor surface where oxidation of organic species can occur. Actually, many reseachers have identified that the p-n junction nanotube catalyst shows a much higher photocatalytic activity than that of TNT catalysts that did not contain a p-n junction [14,114]. Summarily, the main enhancing effect of noble metal loading seems to be a higher rate of production of oxidizing species, but care must be taken to conduct a metal-modified semiconductor with the optimum photocatalytic efficiency.
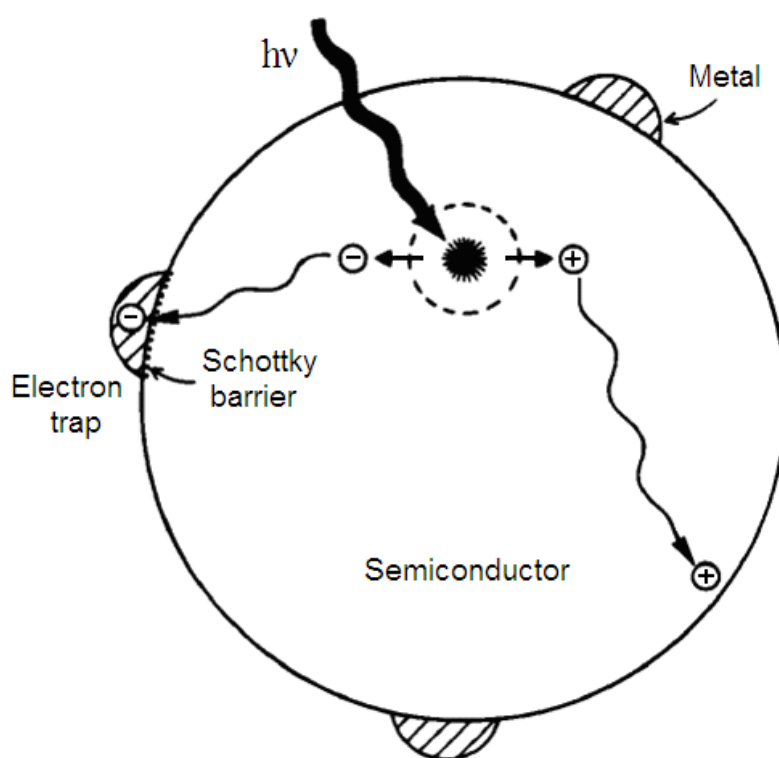

Figure 11. Metal-modified TiO_2 semiconductor photocatalyst particle. Reprinted from ref [4]. Copyright 1995 American Chemical Society.

5.4 Non-metal doping

Earlier studies on TiO_2 particles doped with non-metal atoms, including N, C, F, S and P, etc., have been subject to optical absorption in visible region and visible-driven photocatalytic activity. Asahi and co-workers claimed that among these atoms, the most effective substitutional dopant was N for the bandgap narrowing of TiO_2 [115]. In such doping, the p states (from N dopants) mix with O 2p states (from TiO_2) to narrow the bandgap and then transfer the photogenerated charge carriers to the reactive sites of TiO_2 surface. Although doping by S shows a similar bandgap narrowing, its ionic radius is too big to enable it to be substituted into the TiO_2 lattice [116]. The states introduced by C and P are energetically too deep in the bandgap of TiO_2 to promptly transfer the charge carriers to the surface reactive sites. In F-doped TiO_2 photocatalysts, the main reason for the improved light absorption was the color centers formed upon F incorporation [117].

Although band-gap engineering of TiO_2 particles by non-metal doping has received much attention, doping non-metal atoms into TNTs is quite limited. The preparation methods generally used to form non-metal doped TiO_2 particles, such as high-temperature calcination and chemical vapor deposition, can not been performed to obtain the doped TNTs due to their poor stability. In 2006, Schmuki and co-workers reported the N-doping of anodic TNTs for the first time by N-ion implantation [118] technique and presented a chemically bonded state in $TiO_{2-x}N_x$. Such dopants give rise to the bandgap narrowing by overlapping between N 2p and O 2p orbitals, creation of oxygen vacancies, or generation of intra-bandgap surface states [115,117,119]. It is worth noting that the ion implantation process is often accompanied by undesired radiation defects introduced in the TiO_2, which can act as recombination centres for the photogenerated charge carriers. In the same year, Park et al. [120] reported the carbon doping of the TiO_2 nanotubular layers by reduction of carbon monoxide, where oxygen vacancies were also said to be responsible for the visible-light activity of C-doped TiO_2.

However, in practice, the distribution and amounts of dopants within the TNT materials, which is closely related to the preparation methods, should never be ignored. Too much non-metal atom loading results in the formation of TiN, which is not transparent in the visible region, and more recombination centres, which leads to the poorer photoactivity.

6. Applications of TNT-photocatalysis

The unique physicochemical properties of TNTs, together with their open mesoporous morphology and high specific surface area, make TNTs as photocatalysts very promising for water purification, water-splitting, anti-bacterial/anti-virals, self-cleaning.

6.1 Water purification

TNT is photoactive in the UV region (< 400 nm) and is currently considered one of the most promising photocatalysts for water photocatalytic decontamination due to their high specific surface area and efficient interfacial charge-transfer. Application of TNT-photocatalysis to water purification is expected to destroy the unwanted and harmful organic compounds in contaminated water. In photocatalytic reactions with TNT/UV, two modes of TNT (suspended and immobilized) can be adopted, and dissolved oxygen molecules are considered necessary, TNTs obtained by the hydrothermal and template-assisted methods are usually in a powdery form, and in liquid-soil systems the catalysts require to remove from the treated water. In contrast, TNTs obtained by anodic oxidation are in an immobilized film since they grow directly from the titanium metal substrate. The TNT films used as photocatalysts for the removal of organic and inorganic contaminants in water is coming of age. For example, in 2005 Quan et al. [90]

for the first time employed the TNT film as a photoelectrode to degrade pentachlorophenol in aqueous solution. In 2007, Pan et al. [121] reported the COD removal of landfill leachate solution by using the system of O_3/UV/TNT, where TNTs were prepared by the hydrothemeral method. This could be interesting for industrial applications. In summary, the development of TiO_2 films with large pore morphology, high mechanical robustness, good structural integrity and high surface area, is undoubtedly becoming an important topic in photocatalysis. The system of TNTs combined with other advanced oxidation technologies is potentially applicable to the remediation of industrial effluents, groundwater, surface water and drinking water.

6.2 Water splitting to produce hydrogen

Hydrogen produced from water using solar light is a clean, renewable, and sustainable energy, which will be a critical breakthrough with respect to the rising concern of environmental pollution caused by the use of fossil fuels. Intensive efforts have been made to achieve this goal for the last 30 years. Its technique relies on using a light sensitive material to harness the power of the sun to split water into oxygen and hydrogen gas. Semiconducting materials used as electrodes can absorb solar radiation and make charges, where the charges have energy enough to produce hydrogen. Among them, the TNT array photoanode presents several advantages for the production of molecular hydrogen. For example, (1) due to light scattering within a porous structure, incident photons are more effectively absorbed than on a flat electrode; (2) the tubular nanoarchitecture results in a large effective surface area in close proximity with the electrolyte, thus enabling diffusive transport of photogenerated holes to oxidizable species in the electrolyte; (3) the relevant structure sizes of the TNT arrays, i.e., half the wall thickness, are about 20 nm, which is less than the retrieval length of crystalline

TiO$_2$ [122], hence bulk recombination is greatly reduced and the quantum yield enhances.

Grimes and co-workers first reported the water photocleavage with highly ordered TiO$_2$ nanotube arrays under ultraviolet irradiation [79]. They found that the nanotube wall thickness is a key parameter influencing the magnitude of the photoanodic response and the overall efficiency of the water-splitting reaction. Mohapatra et al. [123] for the first time reported the double-side illuminated TNT arrays for high volume hydrogen generation by water splitting. These double-sided TNT/Ti/TNT materials are used as both photoanode (carbon-doped TiO$_2$ nanotubes) and cathode (Pt nanoparticles dispersed on TNTs; Pt-TNT/Ti/Pt-TNT) in a specially designed photoelectrochemical cell to generate hydrogen by water splitting, as shown in Fig. 12. The experimental results showed that the double-sided TNT photoanode possesses good photoactivity to generate a high volume of hydrogen (38 mL h^{-1}) under the illumination of a solar spectrum on both sides of the photoanode. However, improving the quantum efficiency for photocatalytic water splitting for solar H$_2$ production is still a key research challenge. Reported quantum efficiencies are to date relatively modest.

1. quartz cell, 2. light source, 3. 1M KOH solution containing 5 vol.% ethylene glycol, 4. Ag/AgCl reference electrode, 5. cathode compartment, 6. teflon lid, 7. photoanode containing double sided carbon doped titania nanotubular arrays, and 8. cathode containing platinum nanoparticles and TiO_2 nanotube composites.
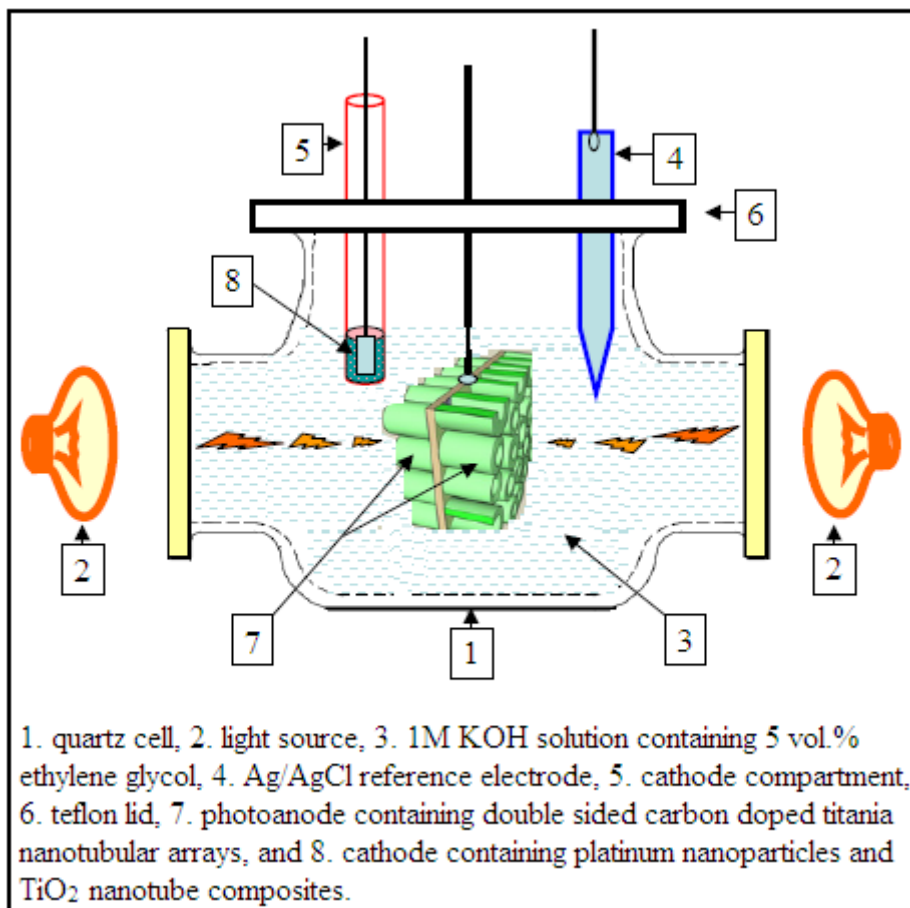
Figure 12. A schematic diagram of the photoelectrochemical cell to generate hydrogen by water splitting using double-side illuminated TiO_2 nanotube arrays. Reprinted from ref [123]. Copyright 2007 American Chemical Society.

6.3 Chemical sensors

Chemical sensors are of critical importance for industrial process control, medical diagnosis, and helping to ensure a safe environment. For example, hydrogen sensors have been widely used in the chemical, petroleum and semiconductor industries, also used as diagnostic tools to monitor certain types of bacterial infections in infants. Since hydrogen has the potential for burning and explosion, sensors are needed to detect hydrogen leaks. However, one problem often found in sensors is that the sensors

become contaminated, or poisoned, limiting their useful lifetime and creating the potential for spurious measurements; typically the more sensitive the sensor, the more susceptible it is to contamination. A sensor need be able to self-clean and recover from environmental insult.

In 2003, Grimes and co-workers reported a self-cleaning, room-temperature TNT hydrogen gas sensor for the first time [124], and the sensor measurement geometry is shown in Fig. 13. This sensor can be able to self-clean with exposure to UV light, fully recovering its initial properties after being contaminated by either motor oil and/or stearic acid. Considering the nature of gas sensing via the interaction of a semiconducting surface with adsorbed gas molecules, it is thought that TNT arrays, with the characteristics of highly ordered open tubes and large specific surface area, can provide abundant sites and channels for gas adsorption, diffusion and chemical reactions. Besides as the hydrogen sensor, anodic TNT arrays have also attracted great interest in their sensing behavior for other gases, such as oxygen, carbon monoxide, carbon dioxide and even ammonia [125-127].
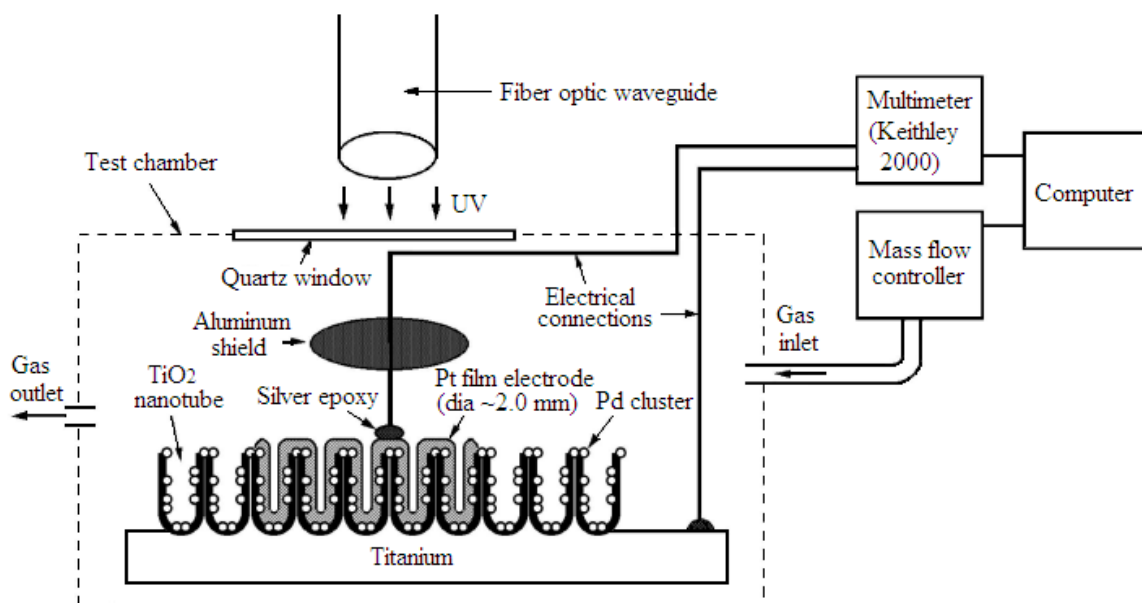
Figure 13. Schematic diagram of experimental geometry used for investigating the self-cleaning capability of the TNT-based room temperature hydrogen gas sensor. Reprinted from ref [124]. Copyright 2003 American Scientific Publishers.

6.4 Anti-bacterial and cancer treatment

Bacterial infection is one of the most common problems after orthopedic implant surgery. If not prevented, bacterial infection can result in serious and life threatening conditions such as osteomyelitis [128]. Thus, antibiotic treatment is usually prescribed to patients to prevent any complications that may arise after implant surgery. In 1985, Matsunaga et al. showed for the first time the ability of UV-irradiated platinized TiO_2 nanopowder to kill bacterial cells in an aqueous environment [129]. Up to 2005, the antibacterial performance of titanate nanotubes was first evaluated by *Escherichia Coli* and *staphylococcus aureus* [130], where the nanotubes were prepared by alkaline hydrothermal method. In 2007, Popat et al. [129] also investigated the ability to control antibiotic release from the anodic TNTs to prevent bacterial adhesion. They demonstrated that nanotubular surfaces enhance matrix production from osteoblasts.

Recently, the feasibility to use the TNT layer as a photocatalyst for the photo-induced cancer cell killing has been investigated [131]. The cancer cells in contact with TNTs can be triggered upon UV light irradiation. Cancer cells reduce their size and a significant amount of them are killed. Furthermore, Sakai et al. [132] found the possibility for selectively killing a single cancer cell using a polarized, illuminated TiO_2 microelectrode. In practice, there are still some problems to be solved before such a device can be put into practical use, because the photocatalytic reactions only occur under UV illumination. Whether the UV light propably causes mutations in normal cells is also unclear and need further study.

7. Conclusions

In this work the pertinent literatures in relation to the scope of TNTs, including the preparation methods, properties, surface modification and photocatalysis applications were compresentively reviewed. TiO_2 nanotubes usually with a large special surface area can be achieved by simple hydrothermal treatment, template-assisted synthesis, or anodic oxidation. Different preparation methods can significantly influence the nanotube morphodology, surface functional groups, even the crystal structures. To effectively utilize the visible light, surface modification of TNTs is usually carried out by sensitizing with dye/polymer molecules, doping with noble metals, and semiconductor coupling. These modifications can dramatically alter the surface and bulk electronic structure, not only offering the advantages of photoresponse to visible light region but the decrease of electron-hole recombination leading to the improvement of photocatalytic efficiency. The employment of these fundamental modification methods is a rich area for both basic scientific research and technological development. Further studies are necessary to elucidate the photocatalytic behavior and mechanism of TNTs for their applications in the fields of water purification, water splitting to generate hydrogen gas, self-cleaning, anti-bacterial, and even cancer cell killing.

References

[1] Hsien, Y.H., Chang, C.F., Chen, Y.H., Cheng, S. Appl. Catal. B-Environ. 2001, 31, 241-249.

[2] Kositzi, M., Poulios, I., Malato, S., Caceres, J., Campos, A. Water Res. 2004, 38, 1147-1154.

[3] Prieto, O., Fermoso, J., Nuĕez, Y., Del Valle, J.L., Irusta, R. Sol. Energy 2005, 79, 376-383.

[4] Linsebigler, A.L., Lu, G., Yates, J.T. Chem. Rev. 1995, 95, 735–758.

[5] Kabra, K., Chaudhary, R., Sawhney, R.L. Ind. Eng. Chem. Res. 2004, 43, 7683-7696.

[6] Li, X.J., Cubbage, J.W., Jenks, W.S. J. Org. Chem. 1999, 64, 8525-8536.

[7] Boer, K W., Survey of Semiconductor Physics. Van Nostrand Reinhold: New York. 1990, p 249.

[8] Mills, A., Hunte, S.L. J. Photochem. Photobiol. A 1997, 108, 1-35.

[9] Hoffmann, M.R., Martin, S.T., Choi, W.Y., Bahnemannt, D.W. Chem. Rev. 1995, 95, 69-96.

[10] Legrini, O., Oliveros, E., Braun, A.M. Chem. Rev. 1993, 93, 671-698.

[11] Konstantinou, I.K., Sakkas, V.A., Albanis, T.A. Appl. Catal. B-Environ. 2001, 34, 227-239.

[12] Ince, N.H., Apikyan, I.G. Water Res. 2000, 34, 4169-4176.

[13] Peng, T.Y., Hasegawa, A., Qiu, J.R., Hirao, K., Chem. Mater. 2003, 15, 2011-2016.

[14] Chen, Y.S., Crittenden, J.C., Hackney, S., Sutter, L., Hand, D.W. Environ. Sci. Technol. 2005, 39, 1201-1208.

[15] Khan, M.A., Jung, H.T., Yang, O.B. J. Phys. Chem. B 2006, 110, 6626-6630.

[16] Mor, G.K., Varghese, O.K., Paulose, M., Shankar, K., Grimes, C.A. Sol. Energy Mater. Sol. Cells 2006, 90, 2011–2075.

[17] Morgado Jr, E., de Abreu, M. A.S., Pravia, O.R.C., Marinkovic, B.A., Jardim, P.M., Rizzo, F.C., Araújo, A.S. Solid State Sci. 2006, 8, 888-900,

[18] Zhang, M., Jin, Z.S., Zhang, J.W., Guo, X.Y., Yang, J.J., Li, W., Wang, X.D., Zhang, Z.J., J. Mol. Catal. A 2004, 217, 203-210.

[19] Du, G.H., Chen, Q., Che, R.C., Yuan, Z.Y., Peng, L.M., Appl. Phys. Lett. 2001, 79, 3702-3704.

[20] Nakahira, A., Kato, W., Tamai, M., Isshiki, T., Nishio, K., Aritani, H. J. Mater. Sci. 2004, 39, 4239-4245.

[21] Ma, R., Fukuda, K., Sasaki, T., Osada, M., Bando, Y. J. Phys. Chem. B 2005, 109, 6210-6224.

[22] Ma, R., Bando, Y., Sasaki, T., Chem. Phys. Lett. 2003, 380, 577-582.

[23] Thorne, A., Kruth, A., Tunstall, D., Irvine, J.T.S., Zhou, W., J. Phys. Chem. B 2005, 109, 5439-5444.

[24] Tsai, C.C., Teng, H.S., Chem. Mater. 2006, 18, 367-373.

[25] Kasuga, T., Hiramatsu, M., Hoson, A., Sekino, T., Niihara, K. Langmuir 1998, 14, 3160-3163.

[26] Kasuga, T., Hiramatsu, M., Hoson, A., Sekino, T., Niihara, K. Adv. Mater. 1999, 11, 1307-1311.

[27] Seo, D.S., Lee, J.K., Kim, H. J. Cryst. Growth 2001, 229, 428-432.

[28] Zhang, Q.H., Gao, L., Zheng, S., Sun, J. Acta Chim. Sinica 2002, 60, 1439-1444.

[29] Zhu, Y.C., Li, H.L., Koltypin, Y., Hacohen, Y.R., Gedanken. A., Chem. Commun. 2001, 24, 2616-2617.

[30] Yang, J.J., Jin, Z.S., Wang, X.D., Li, W., Zhang, J.W., Zhang, S.L., Guo, X.Y., Zhang, Z.J. Dalton Trans. 2003, 3898-3901.

[31] Chen, Q., Du, G. H., Zhang, S., Peng, L.M., Acta Crystallogr. Sect. B 2002, 58, 587-593.

[32] Zhang, S., Peng, L.M., Chen, Q., Du, G.H., Dawson, G., Zhou, W.Z., Phys. Rev. Lett. 2003, 91, 256103.

[33] Yuan, Z.Y., Su, B.L., Colloids Surf. A 2004, 241, 173-183.

[34] Kawai, S., Ueda, R. J. Electrochem. Soc. 1975, 122, 32-36.

[35] Cao, G.Z., Liu, D.W. Adv. Colloid Interface Sci. 2008, 136, 45–64.

[36] Sander, M.S., Cóté, M.J., Gu, W., Kile, B.M., Tripp, C.P. Adv. Mater. 2004, 16, 2052-2057.

[37] Michailowski A., AlMawlawi D., Cheng G.S., Moskovits M., Chem. Phys. Lett. 2001, 349, 1-5.

[38] Martin, C.R. Chem. Mater. 1996, 8, 1739-1746.

[39] Lakshmi, B.B., Dorhout, P.K., Martin, C.R. Chem. Mater. 1997, 9, 857-862.

[40] Zwilling, V., Aucouturier, M., Darque-Ceretti, E., Electrochim. Acta 1991, 45, 921-929.

[41] Gong, D.W., Grimes, C.A., Varghese, O.K., Hu, W.C., Singh, R.S., Chen, Z., Dickey, E.C., J. Mater. Res. 2001, 16, 3331-3334.

[42] Ruan, C.M., Paulose, M., Varghese, O.K., Mor, G.K., Grimes, C.A. J. Phys. Chem. B 2005, 109, 15754-15759.

[43] Wang, J., Zhiqun Lin, Z.Q. J. Phys. Chem. C 2009, 113, 4026-4030.

[44] Cai, Q.Y., Paulose, M., Varghese, O.K., Grimes, C.A., J. Mater. Res. 2005, 20, 230-236.

[45] Paulose, M., Shankar, K., Yoriya, S., Prakasam, H.E., Varghese, O.K., Mor, G.K., Latempa, T.A., Fitzgerald, A., Grimes, C.A. J. Phys. Chem. B, 2006, 110, 16179-16184.

[46] Wang, K.H., Hsieh, Y.H., Wu, C.H., Chang, C.Y. Chemosphere 2000, 40, 389-394.

[47] Chen, Y., Wang, K., Lou, L. J. Photochem. Photobiol. A 2004, 163, 281-287.

[48] Bahnemann, D.W., Kholuiskaya, S.N., Dillert, R., Kulak, A.I., Kokorin, A.I. Appl. Catal. B-Environ. 2002, 36, 161-169.

[49] Yu, J.G., Yu, H.G., Cheng, B., Trapalis, C., J. Mol. Catal. A 2006, 249, 135–142

[50] Li, X.D., Zhang, D.W., Sun, Z., Chen, Y.W., Huang, S.M., Microelectron. J. 2009, 40, 108-114.

[51] Wang, B.Y., Zhang, J.H., Liu, Z.J., Fine Chem. 2003, 20, 333-336.

[52] Kasuga, T., Hiramatsu, M., Hoson, A., Sekino, T., Niihara, K. Adv. Mater. 1999, 11, 1307-1311.

[53] Chien, S.H., Liou, Y.C., Kuo, M.C., Synthetic Met. 2005, 152, 333–336.

[54] Fan, W.G., Gao, L., Zhang, Q.H., Mater. Lett. 2007, 61, 3689-3691.

[55] Imai, H., Matsuta, M., Shimizu, K., Hirashima, H., Negishi. N., Solid State Ionics 2002, 151, 183–187.

[56] Wang, N., Li, X.Y., Wang, Y.X., Quan, X., Chen, G.H., Chem. Eng. J. 2009, 146, 30-35.

[57] Kesselman, J.M., Weres, O., Lewis, N.S., Hoffmann, M.R. J. Phys. Chem. B 1997, 101, 2637-2643.

[58] Turchi, C.S., Ollis, D.F. J. Catal. 1990, 122, 178-192.

[59] Eremia, S.A.V., Chevalier-Lucia, D., Radu, G.L., Marty, J.L. Talanta 2008, 77, 858–862.

[60] Qian, M.L., Zhang, T., Wageh, S., Jin, Z.S., Du, Z.L., Wang, Y.S., Xu, X.R. Nanotechnology 2006, 17, 100–104.

[61] Carp, O., Huisman, C.L., Relle, A., Prog. Solid State Chem. 2004, 32, 33–177.

[62] Burgeois, S., Jomard, F., Perdereau, M. Surf. Sci. 1992, 278, 349-354.

[63] Kim, K.W., Lee, E.H., Kim, Y.J., Lee, M.H., Kim, K.H., Shin, D.W. J. Photochem. Photobiol. A 2003, 159, 301-310.

[64] Janusz, W., Sworska, A., Szczypa, J. Colloids Surf. A 1999, 152, 223–233.

[65] Janusz, W., Galgan, A., Physicochemical Problems of Mineral Processing, 2001, 35, 31-41.

[66] Hunter, R.J. Zeta Potential in Colloid Science; Academic Press: New York, 1981.

[67] Nelson, B.P., Candal, R., Corn, R.M., Anderson, M.A. Langmuir 2000, 16, 6094-6101.

[68] Erdem, B., Hunsicker, R.A., Simmons, G.W., Sudol, E.D., Dimonie, V.L., El-Aasser, M.S. Langmuir 2001, 17, 2664-2669.

[69] Papp, J., Soled, S., Dwight, K., Wold, A. Chem. Mater. 1994, 6, 496-500.

[70] Martra, G. Appl. Catal. A 2000, 200, 275-285.

[71] Boehm, H.P. Angew. Chem. Int. Ed. 1966, 5, 533-544.

[72] Bacsa, R.R., Kiwi, D. Appl. Catal. B-Environ. 1998, 16, 19-29.

[73] Dutta, P.K., Ray, A.K., Sharma, V.K., Millero, F.J. J. Colloid Interf. Sci. 2004, 278, 270–275.

[74] Tokudome, H., Miyauchi, M. Chem. Commun. 2004, 8, 958–959.

[75] Wang, N., Lin, H., Li, J.B., Yang, X.Z., Chi, B. Thin Solid Films 2006, 496, 649-652.

[76] Liang, H.C., Li, X.Z., Yang, Y.H., Sze, K.H. Chemosphere 2008, 73, 805–812.

[77] Tsuchiya, H., Macak, J.M., Ghicov, A., Rader, A.S., Taveira, L., Schmuki, P. Corrosion Sci. 2007, 49, 203–210.

[78] Mor, G.K., Shankar, K., Varghese, O.K., Grimes, C.A. J. Mater. Res. 2004, 19, 2989-2996.

[79] Mor, G.K., Shankar, K., Varghese, O.K., Grimes, C.A. Nano Lett. 2005, 5, 191-195.

[80] Sene, J.J., Zeltner, W.A., Anderson, M.A. J. Phys. Chem. B 2003, 107, 1597-1603.

[81] Zhang, S.M., Chen, Y.Y., Yu, Y., Wu, H.H., Wang, S.R., Zhu, A.L., Huang, W.P., Wu, S.H. J. Nanopart. Res. 2008, 10, 871–875.

[82] Maiyalagan, T., Viswanathan, B., Varadaraju, U.V., Bull. Mater. Sci. 2006, 29, 705–708.

[83] Colón, G., Hidalgo, M.C., Navío, J.A. J. Photochem. Photobio. A 2001, 138, 79–85.

[84] Hong, J., Cao, J., Sun, J.Z., Li, H.Y., Chen, H.Z., Wang, M., Chem. Phys. Lett. 2003, 380, 366–371.

[85] Yang, S.G., Liu, Y.Z., Sun, C. Appl. Catal. A 2006, 301, 284–291.

[86] Lee, S., Jeon, C., Park, Y.C. Chem. Mater. 2004, 16, 4292-4295.

[87] Porkodi, K., Arokiamary, S.D. Mater. Charact. 2007, 58, 495–503.

[88] Takagahara, T., Takeda, K. Phys. Rev. B 1992, 46, 15578-15581.

[89] Monticone, S., Tufeu, R., Kanaev, A.V., Scolan, E., Sanchez, C. Appl. Surf. Sci. 2000, 162, 565-570.

[90] Quan, X., Yang, S.G., Ruan, X.L., Zhao, H.M. Environ. Sci. Technol. 2005, 39, 3770-3775.

[91] Geoffrey, B.S., Thomas, E.M. J. Phys. Chem. B 1997, 101, 2508-2513.

[92] Kim, Y.J., Salim, S., Huq, M.J., Mallouk, T. E. J. Am. Chem. Soc. 1991, 113, 9561-9563.

[93] Macák, J.M., Tsuchiya, H., Ghicov, A., Schmuki, P., Electrochem. Commun. 2005, 7, 1133–1137.

[94] Kang, S.H, Kim, J.Y., Kim, Y., Kim, H.S., Sung, Y.E. J. Phys. Chem. C 2007, 111, 9614-9623.

[95] Liang, H.C., Li, X.Z., Appl. Catal. B-Environ. 2009, 86, 8-17.

[96] Lee, J., Choi, W.Y. J. Phys. Chem. B 2005, 109, 7399-7406.

[97] Kitano, M., Takeuchi, M., Matsuoka, M., Thomas, J.M., Anpo, M. Catal. Today 2007, 120, 133–138.

[98] Chen, S.G., Paulose, M., Ruan, C.M., Mor, G.K., Varghese, O.K., Kouzoudis, D.,

Grimes, C.A. J. Photochem. Photobiol. A 2006, 177, 177–184.

[99] Yin, Y.X., Jin, Z.G., Hou, F. Nanotechnology 2007, 18, 495608.

[100] Hsiao, P.T., Wang, K.P., Cheng, C.W., Teng, H.S., J. Photochem. Photoboiol. A. 2007, 188, 19-24.

[101] Mor, G.K., Shankar, K., Paulose, M., Varghese, O.K., Grimes, C.A., Nano Lett. 2006, 6, 215-218.

[102] Grätzel, M., J. Photochem. Photobiol. C 2003, 4, 145-153.

[103] Zhu, K., Neale, N.R., Miedaner, A., Frank, A.J., Nano Lett. 2007, 7, 69-74.

[104] Salzner, U., Lagowski, J.B., Pickup, P.G., Poirier, R.A., Synth. Metal 1998, 96, 177-189.

[105] Snook, J.H., Samuelson, L.A., Kumar, J., Kim, Y.G., Whitten, J.E., Org. Electron. 2005, 6, 55-64.

[106] Duncan, W.R., Prezhdo. O.V., Annu. Rev. Phys. Chem. 2007, 58, 143-184.

[107] Vogel, R., Pohl, K., Weller, H. Chem. Phys. Lett. 1990, 174, 241–246.

[108] Sant, P.A., Kamat, P.V. Chem. Chem. Phys. 2002, 4, 198–203.

[109] Flood, R., Enright, B., Allen, M., Barry, S., Dalton, A., Doyle, H., Tynan, D., Fitzmaurice, D. Sol. Energy. Mater. Sol. Cells 1995, 39, 83-98.

[110] Guo, Y.G., Hu, J.S., Liang, H.P., Wan, L.J., Bai, C.L., Adv. Funct. Mater. 2005, 15, 196-202.

[111] Hsu, M.C., Leu, I.C., Sun, Y.M., Hon, M.H. J. Cryst.Growth 2005, 285, 642-648.

[112] Lee, J., Choi, W.Y. Environ. Sci. Technol. 2004, 38, 4026-4033.

[113] Könenkamp, R. Phys. Rev. B 2000, 61, 11057-11064.

[114] Han, C.H., Hong, D.W., Kim, J.J., Gwak, J., Han, S.D., Singh, K.C. Sens. Actuat. B 2007, 128, 320–325.

[115] Asahi, R., Morikawa, T., Ohwaki, T., Aoki, K., Taga, Y. Science 2001, 293, 269–271.

[116] Takeshita, K., Yamashita, A., Ishibashi, T., Onishi, H., Nishijima, K., Ohno, T. J. Photochem. Photobiol. A 2006, 177, 269–275.

[117] Zhang, H.J., Chen, G.H., Bahnemann, D.W. J. Mater. Chem. 2009, 19, 5089–5121.

[118] Ghicov, A., Macak, J.M., Tsuchiya, H., Kunze, J., Haeublein, V., Frey, L., Schmuki, P. Nano Lett. 2006, 6, 1080-1082.

[119] Serpone, N. J. Phys. Chem. B 2006, 110, 24287–24293.

[120] Park, J., Kim, S., Bard, A. J., Nano Lett. 2006, 6, 24-28.

[121] Pan, L.M., Ji, M., Wang, M.M., Zhang, X., Lu, B. J. Chem. Ind. Eng. 2007, 11, 2787-2792.

[122] Lubberhuizen, W.H., Vanmaekelbergh, D., Van Faassen, E. J. Porous Mater. 2000, 7, 147-152.

[123] Mohapatra, S.K., Misra, M., Mahajan, V.K., Raja. K.S., J. Phys. Chem. C 2007, 111, 8677-8685.

[124] Mor, G.K.; Varghese, O.K.; Paulose, M.; Grimes, C.A. Sensor Lett. 2003, 1, 42-46.

[125] Varghese, O.K.; Mor, G.K.; Grimes, C.A.; Paulose, M.; Mukherjee, N. J. Nanosci. Nanotechnol. 2004, 4, 733-737.

[126] Wu, M.T., Yao, X., Yuan, Z.H., Sun, H.T., Wu, W.C., Chen, Q.H., Xu, G.Y. Sensor Actuat. B. 1993, 14, 491-494.

[127] Zheng, Q., Zhou, B.X., Bai, J., Li, L.H., Jin, Z.J., Zhang, J.L., Li, J.H., Liu, Y.B., Cai, W.M., Zhu, X.Y. Adv. Mater. 2008, 20, 1044–1049.

[128] Popat, K.C., Eltgroth, M., LaTempa, T.J., Grimes, C.A., Desai, T.A. Biomaterials 2007, 28, 4880–4888.

[129] Matsunaga, T., Nakajima, T., Tomada, R., Wake, H. T. Matsunaga et al., FEMS Microbiol. Lett. 1985, 29, 211-214.

[130] Ling, Y.H., Qi, J.J., Zou, X.F., Zhao, X.M., Bai, X.D., Feng, Q.L., Key Engineering materials. 2005, 280-283, 707-712.

[131] Kalbacova, M., Macak, J. M., Schmidt-Stein, F., Mierke, C.T., Schmuki, P. Phys. Stat. Sol. (RRL) 2008, 2, 194–196.

[132] Sakai, H., Baba, R., Hashimoto, K., Kubota, Y., Fujishima, A. Chem. Lett. 1995, 185–186.